Metal oxide-Graphene oxide nanocomposite thin film for optoelectronic applications

A Synopsis (Approx. 5000 words)

Submitted by

Mrinmoy Chakraborty

In partial fulfillment for the award of degree of

DOCTOR OF PHILOSOPHY

Department of Physics

Presidency University

Kolkata

Registration no:– R-18RS09110167

Email: mrinmoy.rs@presiuniv.ac.in

Date of Registration – 15.11.2019

Under the supervision of

Dr. Sukanta De

Department of Physics

Presidency University, Kolkata

&

Dr. Rabindra Nath Gayen

Department of Physics

Jadavpur University, Kolkata

DECLARATION

I hereby declare that the dissertation entitled "**Metal oxide-Graphene oxide nanocomposite thin film for optoelectronic applications**" to be submitted for the degree of Doctor of Philosophy is my original work and the dissertation has not formed the basis for the award of any degree, diploma, associateship or fellowship of similar other titles. It has not been submitted to any other University or Institution for the award of any degree or diploma.

Place: Kolkata

Date: 28/08/2023

Mrinmoy Chakraborty
(Mrinmoy Chakraborty)

ACKNOWLEDGEMENT

I would like to express my special thanks to my supervisors Dr. Sukanta De and Dr. Rabindranath Gayen for their continuous support and valuable advices to execute these works. I would also like to extend my gratitude to UGC, Govt. of India for providing me fellowship. I would also like to thank my other coauthor E. S. Kadir for his valuable contributions. I also like to thank Department of Physics, Presidency University for providing me this opportunity, numerous facilities and necessary supports to carry out this work. We are also thankful to Indian Association for the Cultivation of Science for FESEM, S. N. Bose National Centre for Basic Sciences (SNBNCBS), Physics Department of Jadavpur University for XRD measurement. We would also like to extend our gratitude to Presidency University for offering infrastructure, basic facilities and necessary supports to carry out this work.

1. Introduction

Wide band gap metal oxide (ZnO, TiO_2, SnO_2 etc.) semiconductors are promising candidates for a wide range of optoelectronics applications such as UV-photodetectors, Dye-Sensitized Solar Cells (DSSCs), chemical sensors and transparent electronics due to their absorption features. They are highly transparent in the visible and near UV-light region, environmental friendly, as well as thermally and chemically stable [1]. Among them, Titanium dioxide (TiO_2) is an exceptionally multi-skilled material as it can be utilized in a variety of optoelectronics applications, including self-cleaning surfaces [2], dye sensitized solar cells [3-5], photo-catalysis [6-7] and photo-sensors/photodetectors [8-9]. TiO_2 nanoparticles are the most efficient metal oxide photo-anode of dye-sensitized solar cells (DSSCs) due to its wide band gap (3.2 eV), outstanding chemical stability, high excitonic binding energy, higher electron mobility, thermal stability, low-cost and non-toxicity [10-12]. Moreover, TiO_2 is an exceptionally stable material, which is extremely photoactive and stable under UV irradiation due to its band gap, has recently been used to make the most consistently used UV sensors. Zinc oxide (ZnO) is another promising and attractive low-cost porous semiconductor material possessing prominent photoconductivity in the UV region of the electromagnetic spectrum because of its wide band gap (3.3 eV at RT) with high sensitivity in adsorbing oxygen on the surface and large excitonic binding energy (60 meV) at room temperature [13]. ZnO has non-toxic and higher photocatalytic efficiency with good sensing behaviour and excellent thermal, mechanical and chemical stability [14]. As one of the multi-skilled electronic and photonic material, ZnO exhibits promising applications in optoelectronics devices because of their unique and optical properties [15]. Also, ZnO has higher excitonic electron mobility (~115 $cm^2\ V^{-1}\ s^{-1}$), longer electron lifetime and stability against photo-corrosion, which makes it the most efficient photo-anode for DSSCs applications [16]. So, ZnO is promising for a broad range of optoelectronics applications such as UV-light emitter or UV-detector, chemical sensor, DSSC and transparent electronics. But the efficiency of the devices based on these oxide semiconductors, with its various microstructures in low dimensions and the photovoltaic performance is still relatively low compared to other photo-anode in photovoltaic applications, is hindered by slow response and weak photo-responsivity due to fast recombination of the photo-generated electron-hole pairs [14]. Also, there is a tendency for charges to be accumulated rather than transported at those grain boundaries induced potential barriers, which obstruct the transportation of charge carriers inside the materials, resulting in poor electrical conductivity of the metal oxide thin films [17]. In these sense, researchers have tried many different methods such as doping process, different production methods, coupling of other semiconductors, especially a heterojunction based on based on two different kinds of semiconductors with different energy band structures to improve the photoconductivity through i) the enhanced separation of photo-generated electrons and holes on the metal oxide surface which is turn effectively slows down the recombination rate, ii) the modification of carrier transport by introducing

conductive frameworks in the host oxide matrix [15,18]. In recent times, several efforts have been made to solve this issue by combining metal oxide with other functional materials like graphene, reduced graphene oxide (rGO) or GO [19]. Graphene is a unique transparent 2D material made of sp^2–carbon atoms arranged in hexagonal network with remarkable electrical, mechanical and optical properties which becomes more reactive when oxidized [20-21]. Recently, graphene and its functionalized and/or composite materials are being extensively researched owing to their high active surfaces and excellent carrier mobility besides other unique properties [22]. GO contains a mixture of sp^2 and sp^3 hybridized carbon atoms which are attributed to the creation of new sp^2 clusters by removing the oxygen atoms which provide easy reduction pathway [23]. All such helpful properties of GO make it a suitable candidate to be used as a dopant. Therefore, TiO_2-GO and ZnO-GO composite material may be a very promising contender for a wide range of optoelectronic applications. There have been a number of reports based on ZnO-GO or TiO_2-GO UV photodetector and also graphene oxide composited ZnO or TiO_2 nanocomposites thin film as highly efficient photo-anode for dye-sensitized solar cells. There are so many reports related to high performance UV photodetector based on TiO_2/ZnO heterojunction and also ZnO NW-TiO_2 thin films based electrodes used as an efficient photo-anode for dye-sensitized solar cells to improve the photovoltaic properties. Due to huge surface to volume ratio, ZnO nanowires exhibit significant sensitive photo-responsive behaviour under UV irradiation via electron-hole production compared to other nanostructures [24-26]. Thus ZnO NWs possess better sensitivity along with faster response for optical communications [27-28]. The nanowire assembly also provide a very large surface area for the adsorption of the dye, which ultimately increase the photo-current and hence the power conversion efficiency (PCE) efficiency of the DSSCs. Further, a thin-layer of TiO_2 over the nanowire assembly increase the dye absorption surface area as well as protect the unstable ZnO nanowires from etching away in the dye and electrolyte solution. These thin films are more efficient photo-anode with high transparency enhanced photo current and resulted in considerable improvement in efficiency. So, a hybrid nanostructure combining nanowire and nanoparticles with GO can improve the power conversion efficiency of DSSCs where larger effective surface area of nanoparticles enhances dye loading capacity and nanowires facilitate better charge transport [29-30]. So, hybrid nanostructure combining nanowire and nanoparticles with GO generates the built-in electric field and provides more efficient charge separation which can increase the number of charge carriers, carrier lifetime and ultimately improves the performance of optoelectronics devices.

Here we discussed in detail synthesis and characterizations of highly transparent metal oxide (ZnO, TiO_2, etc.)-graphene oxide nanocomposites by sol-gel spin coating technique. The modulation of the microstructural, optical and electrical properties of the individual metal oxide semiconductors as well as hybrid nanostructures with the GO incorporation were studied thoroughly. To understand the charge transport mechanism in connection with the grain boundary modification in the nanocomposite thin films

were studied by DC bias dependent impedance spectroscopic measurements. Enhanced UV photo-response properties of the individual metal oxide semiconductors as well as the hybrid nanocomposite thin films with GO were studied by UV photoconductivity measurements. High transparency with enhanced photo current makes TiO_2-GO, ZnO-GO, hybrid TiO_2-ZnO NW-GO and hybrid ZnO NW-TiO_2-GO nanocomposite thin films more efficient photo anode for Dye-Sensitized Solar Cells (DSSCs).

2. Literature review

Optoelectronics devices such as light emitting diodes (LEDs), photodiodes, Dye-Sensitized Solar Cells (DSSCs) based on metal oxide-graphene oxide (GO) nano-composites play an important and expanding role in modern day technology. Among them, UV photo-detectors based on wide band gap metal oxide (ZnO, TiO_2, V_2O_5, etc;) – graphene oxide nano-composites have been researched extensively because they are easy to manufacture, economical and highly responsive/sensitive in the UV region [31]. In this review, we highlight the latest literature with a clear focus on graphene-based metal and metal oxide nano-composites for optoelectronics applications. It has been proved that the photocatalytic activity of TiO_2/rGO and ZnO/rGO were several times higher than pure TiO_2 and pure ZnO respectively [32-33]. To improve the performance of the UV photo-detector, different types of variations of nanomaterial based UV photo-detectors have been developed, such as metal-semiconductor-metal (MSM) structure [34], schottky photo barrier photodiodes [35], and composite with organic materials [36]. Reports also suggests that with inclusion of GO or rGO with ZnO and TiO_2 shows an enhancement of the photo-responsivity, detectivity and photo-sensitivity in comparison to pure TiO_2 and pure ZnO. Also the response time and recovery time are much more smaller for TiO_2/rGO and ZnO/rGO as compared to that of pure TiO_2 and pure ZnO [14,31]. Very recently, (S. Mahaliangam et al; 2022) reported on ZnO/GO nanocomposites as efficient photoelectrode in DSSC, where relatively high power conversion efficiency has been obtained for ZnO/GO nanocomposites as efficient photoelectrode in DSSC than pure ZnO thin film based DSSC. This is due to the greater specific surface area of GO, high electron mobility of ZnO, less electron-hole recombination and the two-dimensional graphene oxide composited ZnO enabled efficient charge transfer in the DSSCs, resulting in improved performance [37]. Also, highly transparent graphene oxide composited TiO_2 thin film was used as a efficient photo-anode for DSSCs in comparison to pure TiO_2 thin film based DSSCs. This is due to the modification of grain boundaries for facilitating the charge transport instead of accumulation which results in decrease of recombination and increase of lifetime of photo-generated charge carriers of host matrix with enhanced photocurrent. Thus, the overall power conversion efficiency (η) increased significantly with the use of TiO_2-GO nanocomposite thin films as DSSC photo-anode instead of pristine

TiO_2 thin film [38]. Also researchers have paid more attention to the couple of semiconductors including GO with different energy band structures like ZnO NW-TiO_2-GO, TiO_2-ZnO NW-GO, etc. to improve the optoelectronics applications due to their outstanding optoelectronics characteristics. (D. Zhang et al; 2015) reported about the high performance UV detector along with high responsivity based on TiO_2/ZnO heterojunction compared with the Pure TiO_2 or pure ZnO thin film. This is due to the fact that the built-in electric field in the heterojunction has been generated and provides more efficient charge separation which can result in a growth in the number of carriers [15].

3. Synthesis, characterizations and optoleectronic applications of TiO_2-GO thin films

3.1. Synthesis of TiO_2-GO thin film

TiO_2 – GO nanocomposite thin films were synthesized on FTO coated glass substrates by sol-gel spin coating technique by previously reported method [39]. To prepare the TiO_2 solution, we follow the method developed by Vasuki et al; [40]. At first, 5 ml of pure ethanol (Merck, purity >99%) was taken in a small conical flask to mix with 1.5 ml of Titanium IV-Isopropoxide (TTIP) (Sigma-Aldrich, purity> 99.9%). After stirring this solution by a magnetic peddle using a magnetic stirrer for 15 minutes at room temperature, 0.5 ml (8 drops) of Di-ethanolamine (DEA) (Merck, 98%) was added into this solution. After another 15 minutes of vigorous stirring, 5 ml of pure ethanol (Merck, purity >99%) was mixed bringing the total volume ratio of each ingredient (TTIP, DEA and Ethanol) in the solution was calculated to be 3:1:20. Now after 1.5 hours of constant stirring at room temperature, we finally got the homogeneous and transparent TiO_2 solution. To produce the Graphene Oxide (GO) solution, 2 mg of graphene oxide powder [41] was taken in a beaker to mix with 50 ml of isopropanol (Merck, 99%), followed by ultrasonication for 6 hours. Finally, the solution was filtered, and the resulting solution was stored as a clean and transparent GO solution. After that, the solution of TiO_2 and the solution of GO were mixed in the suitable volume ratio to obtain TiO_2-GO (5%), TiO_2-GO (10%) and TiO_2-GO (15%) solutions. The TiO_2 solution and TiO_2-GO solution were then spin-coated using the manually programmed spin –coater (spinNXG M-1 spin-coater) on FTO-coated glass substrates at 3000 rpm for 30 secs, followed by drying at 393 K for 10 mins in the hot air oven. Finally, these compounds were annealed at 673 K for 1 hour to obtain TiO_2 and TiO_2-GO composite thin films and stored in vacuum desiccator for further analysis.

3.2. Microstructural studies

Fig. 1 displays the surface morphology of both pure TiO_2 and TiO_2-GO nanocomposite thin film at a concentration of 10 % GO. As can be seen from the surface morphology, the TiO_2 thin film (Fig. 1(a)) is made up of nanocrystalline grains that are distributed uniformly and tightly packed in their natural state. When there is 10 % GO present in the host TiO_2 matrix (Fig. 1(b)), only a small quantity of GO flakes can

be seen on the surface. The well-dispersed nature of GO inside the nanocomposite may be confirmed by the relatively smooth nature of the majority of the surface area, which ultimately alters the inter-grain or grain boundary regions.

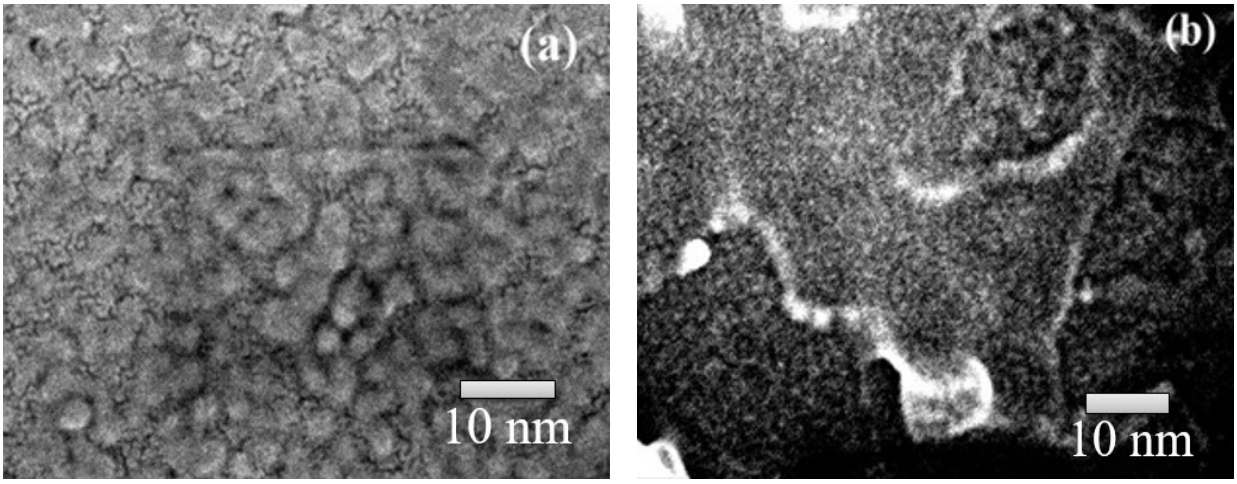

Fig. 1. The FESEM picture of a thin film is made up of (a) TiO_2 and (b) TiO_2-GO at a concentration of 10 %.

The XRD patterns of thin films composed of TiO_2 and TiO_2-GO nano-composites at 5%, 10%, and 15% concentrations are shown in fig. 2. Both the tetragonal anatase phase and the tetragonal rutile phase of TiO_2 are present in thin films, as shown by the XRD patterns. The rutile phase of TiO_2 is responsible for the

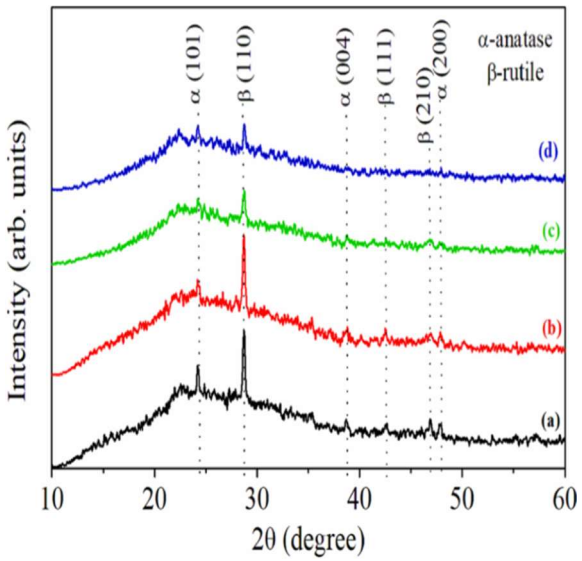

Fig. 2. The XRD pattern of thin films is made up of (a) TiO_2, (b) TiO_2-GO (5%), (c) TiO_2-GO (10%), and (d) TiO_2-GO (15%).

observation of a significant diffraction peak (JCPDS card no. 21–1276) that is caused by reflection from the (110) plane, and very minor peaks that are caused by reflection from the (111) and (220) planes can also be seen. Along with smaller peaks that are caused by reflection from (004) and (200) planes.

3.3. Impedance analysis

At room temperature, bias dependent impedance spectroscopy measurements were carried out in the frequency range of 4 Hz - 5 MHz in order to get the information regarding the conduction process. The complex impedance, denoted by Z, may be expressed in mathematical form as:

$$Z = Z' + jZ'' \qquad \ldots\ldots\ldots\ldots\ldots\ldots \quad (i)$$

Using impedance spectroscopic data imaginary part of complex impedance (Z'') with real part of it (Z') known as Nyquist plots are plotted at various external bias condition for TiO_2 and its nano-composites are shown in fig. 3 (a-d). Because of the reduction in impedance, the arcs of the semi-circles of the Nyquist plots exhibit a falling trend when the external bias voltage is increased for all of those samples, suggesting grain-boundary modification occurs when an external field is applied. Also increase in concentration in GO fraction reduces the arcs of those semi – circles. The variations of relaxation times τ_1 and τ_2 can be caused by an external bias voltage for TiO_2-GO nano-composite thin films as shown in the insets of fig. 3 (a-d). Here, τ_1 and τ_2 denote the relaxation times that may be associated with the contribution of grains and grain boundaries of the nano-composites, respectively. In order to get their values of τ_1 and τ_2, one must first ensure that the Nyquist plot is properly fitted with an appropriate electrical model circuit.

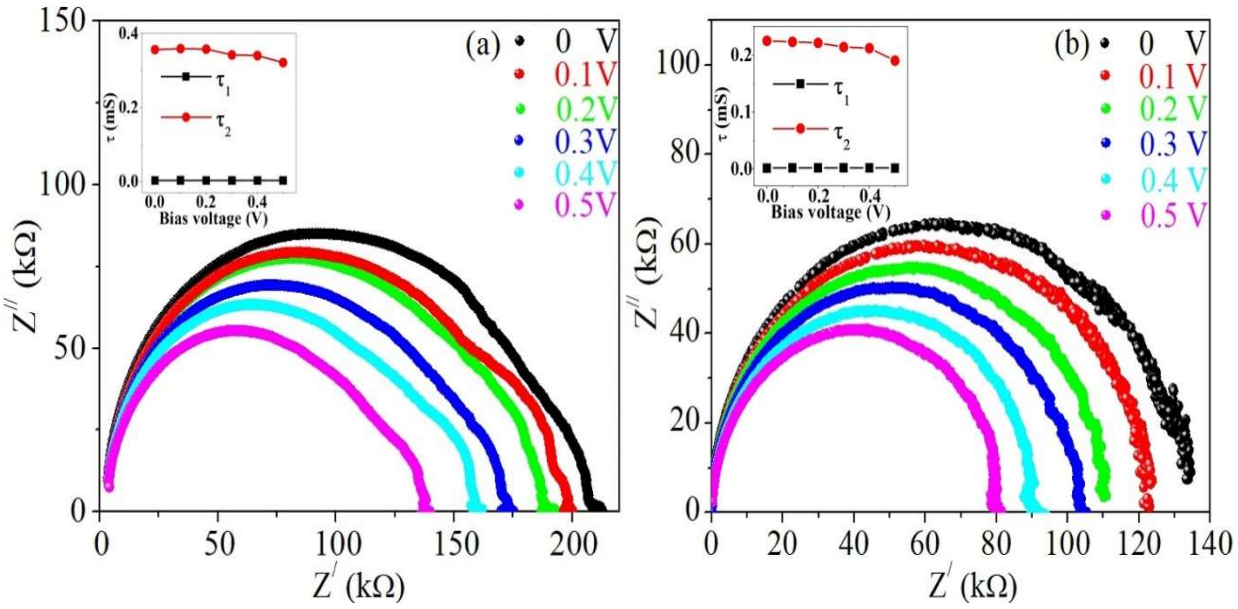

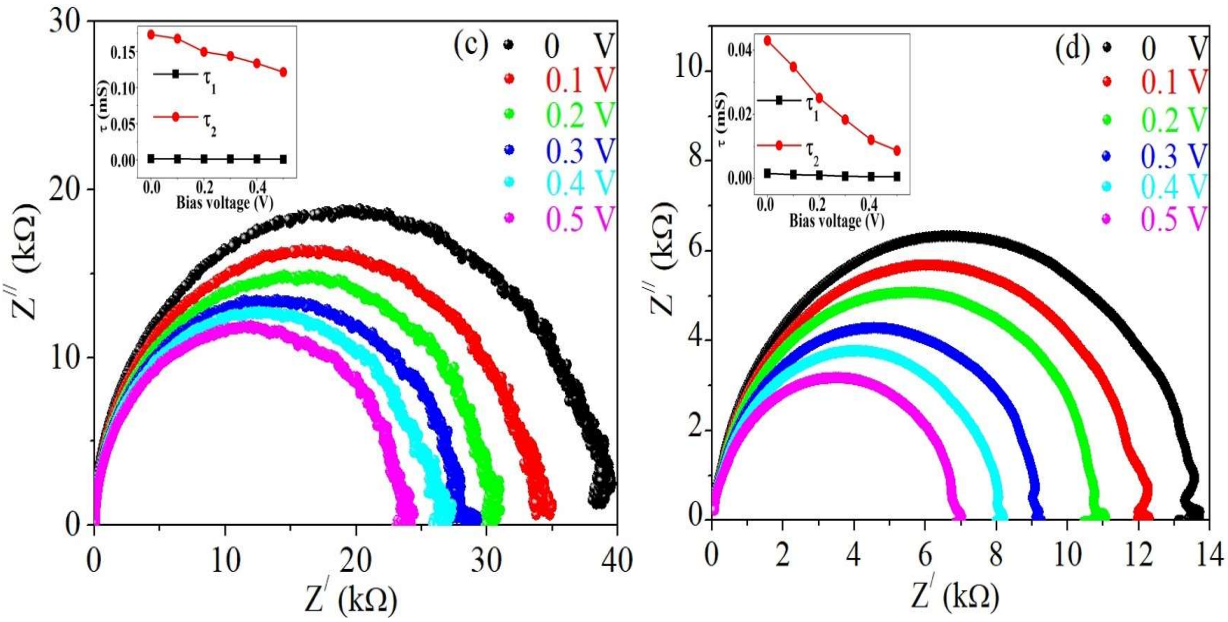

Fig. 3. Nyquist plot ($Z^{//}$ vs $Z^{/}$) as a function of DC bias and the change of τ_1 and τ_2 with external DC bias (inset) for (a) pure TiO_2, (b) TiO_2-GO (5%), (c) TiO_2-GO (10%), (d) TiO_2-GO (15%), respectively.

Electrical model circuit consisting of two parallel R - C circuit and a series resistance R_s are used to fit experimentally acquired Nyquist plots in order to properly evaluate the conduction phenomena in those nano-composites, and separate out the involvement of grain and grain-boundaries in TiO_2 and its nano-composites. Under the influence of a tiny ac signal, relaxation times, denoted by the equation ($\tau = RC$), resulting from the various electrical responses are analyzed and determined. By fitting a Nyquist plot, the EIS spectrum analysis software was able to calculate the resistances and capacitances of this modelled circuit [42]. A variety of electrical characteristics such as R_s, R_1, R_2, C_1, C_2 are determined as fitting parameters and the relaxation times (($\tau_1 = R_1C_1$), ($\tau_2 = R_2C_2$)) distributions are calculated for different composites and are tabulated in Table I. A further observation that has been made arising from the changes of relaxation times τ_1 and τ_2 with external dc bias voltage (insets of Fig. 3 (a-d)). It has been observed that there is no such variation occurs in τ_1 in all films with external bias voltage, which is assumed to be the contribution of core grains. This is because of external bias not effecting polarization the grains. On the other hand, since τ_2 is the relaxation behavior of grain boundaries or interfaces, the external bias voltage has a considerable effect on it.

Table-I: Values of resistors (R), Capacitors (C) obtained as fitting parameters and time constants (τ) for TiO_2 and TiO_2-GO composite thin film**.**

Film Name	R_s (Ω)	R_1 (Ω)	C_1 (F)	R_2 (Ω)	C_2 (F)	$\tau_1 = R_1C_1$ (sec)	$\tau_2 = R_2C_2$ (sec)
TiO_2	0.89	11892	2.66×10^{-10}	103930	3.42×10^{-9}	3.16×10^{-6}	3.56×10^{-4}
TiO_2-GO (5%)	3.19	50585	3.36×10^{-11}	338080	6.67×10^{-10}	1.70×10^{-6}	2.25×10^{-4}
TiO_2-GO (10%)	1.02	1965	8.56×10^{-10}	35762	4.85×10^{-9}	1.68×10^{-6}	1.73×10^{-4}
TiO_2-GO (15%)	33.72	475.12	3.37×10^{-9}	29862	1.44×10^{-9}	1.60×10^{-6}	4.30×10^{-5}

3.4. Dye-sensitized solar cells

The illuminated J-V curves for the TiO_2, and TiO_2-GO (10 %) photo-anode based DSSC structures are shown in Fig. 4(a) and Fig. 4(b), respectively. A conventional DSSC structure is fabricated consisting of this hybrid structure as photo-anode, ruthenium based N3 dye as photosensitizers, iodine solution (I-/I3+) as electrolyte and fluorine-doped tin oxide (FTO) coated glass substrate as counter electrode. From the J-V characteristics curve under illumination, the open circuit voltage (V_{oc}) and short-circuit current density (J_{sc}) of TiO_2 based DSSC are ~ 435 mV and ~ 0.50 mA/cm^2, respectively. When the GO content in the nanocomposite thin films is increased to 10 %, the values of V_{oc} and J_{sc} reached to 469 mV and 1.89 mA/cm^2, respectively (Fig. 4(b)). The V_{oc}, J_{sc} and η values for a variety of samples are presented in Table-II. The power conversion efficiency (η) of TiO_2 photo-anode based DSSC is calculated as 0.07 % which enhanced to 0.26% for TiO_2-GO (5%) nanostructured photo-anode based DSSC. In the TiO_2-GO (10%) based DSSC structure, the maximum value of power conversion efficiency (η ~ 0.48 %) is obtained.

TABLE- II: Characteristic parameters of different photo-anode based DSSCs estimated from J-V curves

DSSC Photo-anode	J_{SC} (mA/cm^2)	V_{OC} (mV)	FF	η (%)
TiO_2	0.50	0.435	0.32	0.07
TiO_2-GO (5 %)	1.65	0.467	0.34	0.26
TiO_2-GO (10 %)	1.89	0.469	0.55	0.48

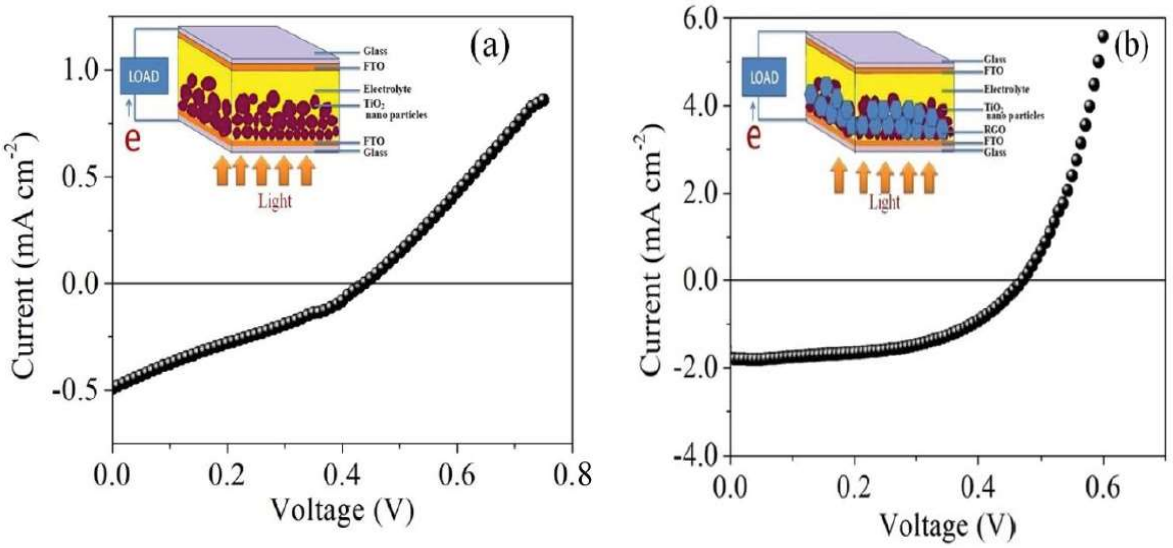

Fig. 4. The J-V curves during illumination for the DSSC based on (a) pure TiO_2 photo-anode and (b) TiO_2-GO (10%) photo-anode; Inset shows the Schematic illustration of the corresponding devices.

3.5. UV Photodetector

Fig. 5 (a-b) shows the time-dependent UV induced photo-responses of TiO_2 and TiO_2-GO (5%) nano-composites, which were investigated by exposing them to UV light with a wavelength of 365 nm and a power of 8.07 μW. Both the dark and the UV photocurrent are shown to rises continuously when GO is gradually incorporated into the TiO_2 material. This is due to the fact that the establishment of GO

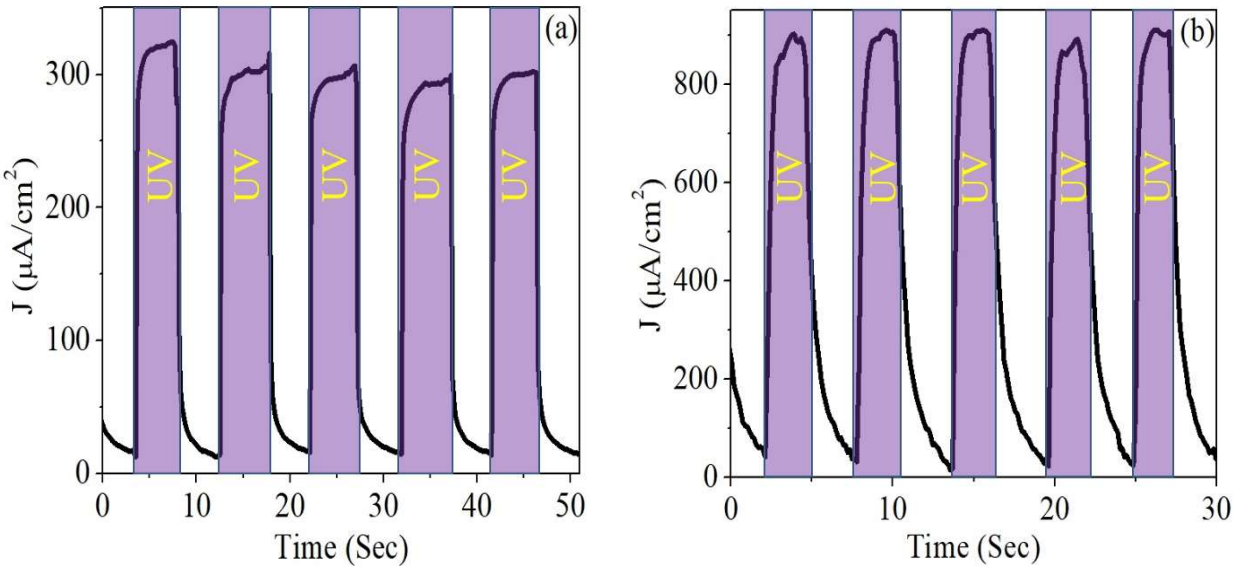

Fig. 5. Time dependent UV induced photo responses of thin films made of (a) TiO_2 and (b) TiO_2-GO (5%) nanocomposite thin films

conducting networks extends the lifetime of photo-generated charge carriers and performs as a transport layer between the conduction band of TiO_2 and the acceptor electrode as a result of its ability to lower the recombination loss [43]. Table III presents the results of measuring the dark and UV photocurrents of several composites of TiO_2 thin films.

Table – III: Different parameters of Pure TiO_2, TiO_2-GO (5%), TiO_2-GO (10%) and TiO_2-GO (15%) thin films.

Sample	Dark current density (mA/cm^2)	Photo current density (mA/cm^2)	Response current Density (mA/cm^2)	Response time (Sec)	Recovery time (Sec)
TiO_2	0.01	0.32	0.31	1.15	1.48
TiO_2-GO (5%)	0.04	0.91	0.87	0.88	1.07
TiO_2-GO (10%)	0.07	1.35	1.28	0.50	0.76
TiO_2-GO (15%)	0.09	1.87	1.78	0.28	0.41

Fig. 6 (a-d) shows the Nyqust plot obtained from experimental impedance spectra along with fitted Nyquist plot where EIS spectrum analysis software [44] was used to fit these experimental Nyquist plots using a suitable electrical model circuit (inset of Fig. 6(a-d)) consisting of a series resistance that is connected in series with two parallel R-C circuits. The impedance spectra were measured under dark and under UV illumination. Table IV shows the values of the resistors and capacitors that were used as fitting parameters. One of these characteristic parameters, R_1, is recognized as the transport resistance of core grains, while another, R_2, is identified as recombination resistance or transfer resistance related to the rate of electrons recombining at the conduction band [45]. R_2 is supposed to represent the contribution that arises out of those boundaries due to the fact that recombination occurs more often near the boundaries and interfaces, which serve as recombination centers [46]. Under the influence of UV irradiation, transport resistance R_1 drops dramatically as a result of photo excitation of electrons. However, under UV irradiation, the decrease in the values of R_2 is caused by the diffusion of photo-generated charge carriers to the boundaries. Recombination resistance or transfer resistance (R_2) decreases progressively with the incorporation of GO at the boundaries, which results in a lesser probability that photo-generated charges would get trapped [47].

This long-lived extra charge carrier enhances the photo-responsive properties of nano-composite thin films. The relaxation times, represented by the equation ($\tau = RC$), may be determined using these values for the various regions of electrical responses. The contribution of interfacial or space charge polarization is expressed as the time constant with a greater value, denoted by τ_2 ($=R_2C_2$), whereas the contribution of dipolar or orientational polarization of core grains is supposed to be represented by the smaller time constant, denoted by τ_1 ($=R_1C_1$). After the integration of GO into the host nanomaterial, the change in τ_2 is considerably larger compared to that of τ_1, showing that the interfaces at the boundaries have been modified. When these composites are exposed to UV light, the relaxation times consistently decrease, which indicates easy relaxation of dipoles associated with increased UV photoconductivity.

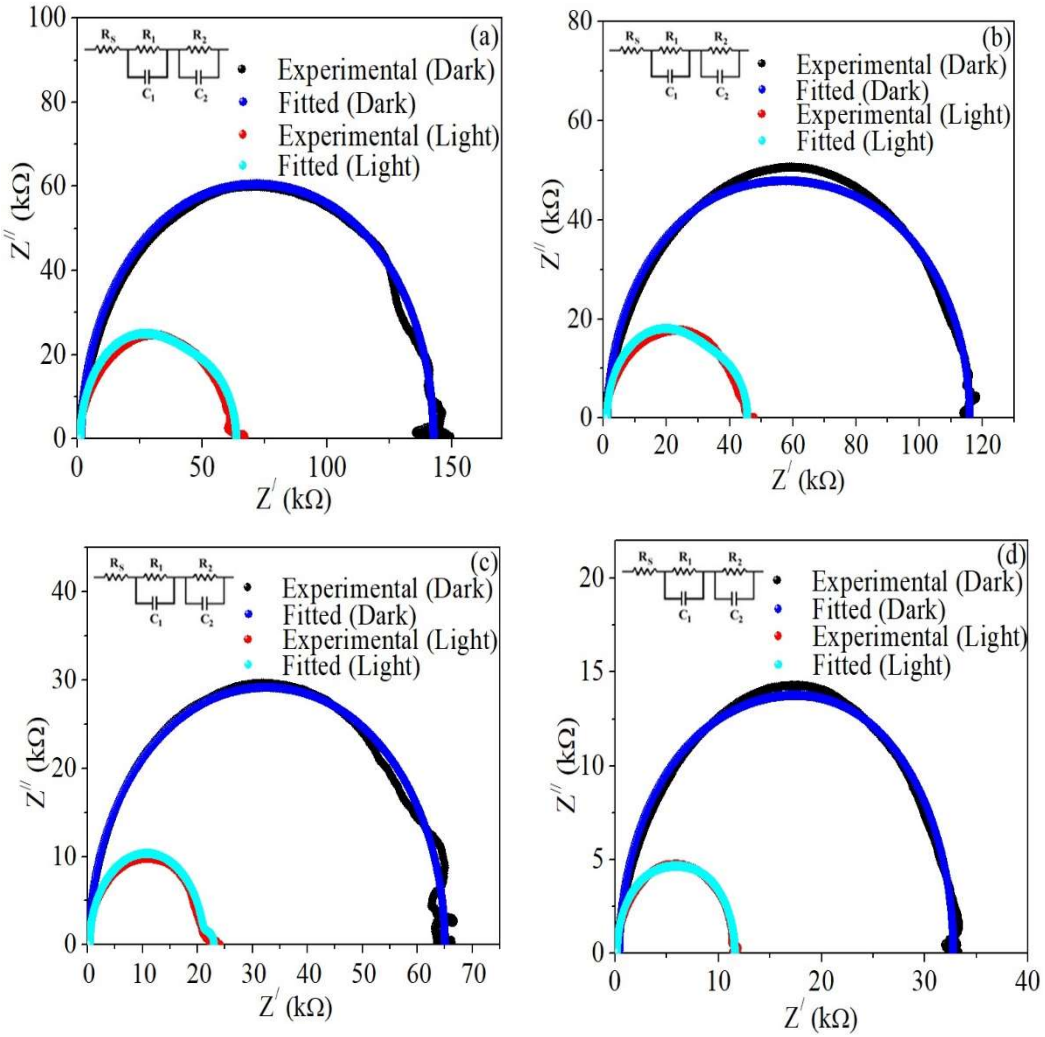

Fig. 6. Experimentally produced Nyquist plots with fitted curves for (a) Pure TiO_2, (b) TiO_2-GO (5%), (c) TiO_2-GO (10%), and (d) TiO_2-GO (15%) thin films conditions under dark and UV conditions.

Table –IV: Different parameters determined by the EIS spectrum analysis software using the fitted Nyquist curves

Film	R_S (Ω)	R_1 (Ω)	R_2 (Ω)	C_1 (F)	C_2 (F)	τ_1 ($R_1 \times C_1$) (sec)	τ_2 ($R_2 \times C_2$) (sec)	Error (%)
TiO_2 (Dark)	1207.4	73285	68548	2.16×10^{-10}	1.16×10^{-9}	1.58×10^{-5}	7.96×10^{-5}	1.38
TiO_2 (UV)	1201.7	20500	41861	7.56×10^{-10}	1.18×10^{-9}	1.55×10^{-5}	4.94×10^{-5}	1.24
TiO_2-GO (5 %) (Dark)	858.8	60930	53932	2.45×10^{-10}	1.15×10^{-9}	1.49×10^{-5}	6.23×10^{-5}	1.38
TiO_2-GO (5 %) (UV)	873.5	16793	27615	7.78×10^{-10}	1.22×10^{-9}	1.31×10^{-5}	3.36×10^{-5}	1.37
TiO_2-GO (10 %) (Dark)	641.9	33958	30664	3.37×10^{-10}	1.74×10^{-9}	1.14×10^{-5}	5.34×10^{-5}	0.76
TiO_2-GO (10 %) (UV)	376.6	10619	19933	7.24×10^{-10}	14.4×10^{-9}	7.69×10^{-6}	2.87×10^{-5}	2.03
TiO_2-GO (15 %) (Dark)	404.1	13592	18774	2.91×10^{-10}	0.7×10^{-9}	3.96×10^{-6}	1.31×10^{-5}	0.84
TiO_2-GO (15 %) (UV)	161.8	5632	5786	5.04×10^{-10}	1.83×10^{-9}	2.84×10^{-6}	1.06×10^{-5}	0.41

4. Fabrication of TiO_2-GO coated vertically aligned ZnO nanowire for DSSC applications

4.1. Synthesis of ZnO NW/TiO_2-GO thin film

Vertically well aligned ZnO nanowires were synthesized by a two-step chemical technique onto properly cleaned fluorine doped tin oxide (FTO) coated glass substrates. At first, nanocrystalline ZnO seed layers were deposited on FTO coated glass substrates by sol-gel spin coating technique. The ZnO solution was prepared by mixing zinc acetate in isopropyl alcohol along with appropriate amount of diethanolamine [48]. This solution was then drop-casted on cleaned FTO coated glass substrate by a manual programmed spin coater (Apex instrument - Spin NXG-M1 spin-coater) at a speed of 3000 rpm for 1 minute, followed by drying at 393 K for 10 mins in the hot air oven. Finally, these films were annealed at 673 K for 1 hour to achieve uniformly distributed ZnO nanocrystalline seed layers. Well aligned ZnO nanowires were grown in a chemical bath containing aqueous solution of Zinc nitrate hexahydrate ($Zn(NO_3)_2.6H_2O$) (Sigma Aldrich, 98%) and (NaOH) Sodium hydroxide pellets (Merck, extrapure) in 1:40 molar ratio. For this, 0.15 gm of Zinc nitrate hexahydrate ($Zn(NO_3)_2.6H_2O$) (Sigma Aldrich, 98%) was dissolved in 50 ml of distilled water. 0.8 g of NaOH (Sodium Hydroxide pellets) (Merck, extrapure) was added to this solution, so that the ratio of ($Zn(NO_3)_2.6H_2O$) :NaOH = 1:40. As, the temperature of the solution was increased upto 343 K,

the FTO-coated glass substrates with 2-3 pre-deposited ZnO seed layers were immersed vertically into the solution. This solution was continuously stirred (Labman Hotplate Magnetic Stirrer) slowly for 1 hour with a magnetic peddle at 343 K. After 1 hour of deposition, the films were taken out of bath and washed by trickling distilled water from back to wash away any unwanted sediment. Finally, these films containing vertically well aligned ZnO nanowire were dried in a hot air oven at 393 K for 10 minutes. To fabricate the hybrid nanostructure, TiO_2-GO nanocomposite thin films were made on top of vertically well aligned ZnO nanowires by similar previously reported sol-gel spin coating technique [49]. The process of making the mixed (TiO_2-GO) solution has previously been discussed in detail. Finally, these mixed solutions were then spin coated onto the vertically well aligned ZnO nanowire at 3000 rpm for 30 s using a manual programmed spin coater (Apex instrument - Spin NXG-M1 spin-coater). The obtained layer was then dried at 393 K for 10 minutes between successive depositions in the hot air oven. Finally, these compounds were annealed at 673 K for 1 hour to obtain hybrid ZnO nanowire-TiO_2-GO nanocomposite thin film and stored in vacuum desiccator for further analysis.

4.2. Microstructural Studies

Fig. 7 shows the FESEM images of ZnO NW and a representative ZnONW/TiO_2-GO thin film with 5% GO, along with inset showing a cross-sectional view of the corresponding film. From the top view of the FESEM images, it is clear that the top of the ZnO NWs as well as the inter nanowire pores gets covered due to coating. The thicknesses of the films are determined using the cross-sectional view of the FESEM images, as shown in the inset of Fig. 7.

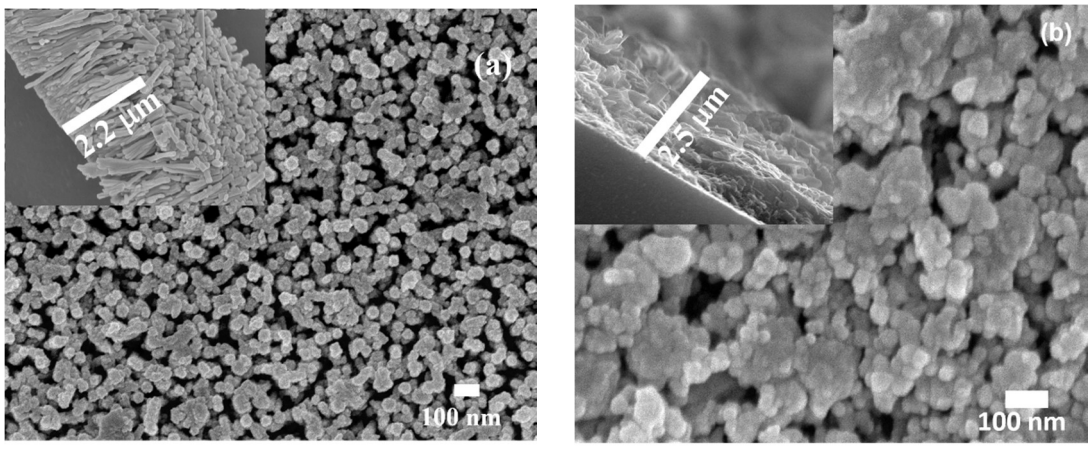

Fig. 7. The FESEM image of (a) ZnO NW and (b) ZnO NW/TiO_2-GO (5 %) thin film (Inset: Cross-sectional image).

Fig. 8 (a) depicts the XRD pattern of ZnO nanowire thin films that were deposited on glass substrates. This pattern exhibits the diffraction peaks that may be ascribed due to the reflections from the (100), (002), (101), (102), and (110) crystal planes of wurtzite ZnO (JCPDS 36-1451). The XRD pattern for pure TiO_2 thin films reveals the formation of the β phase of rutile TiO_2 (JCPDS 21-1276), as seen by the appearance of a corresponding diffraction peak caused by reflection from the (110) plane (Fig. 9(b)). The XRD patterns of a hybrid ZnO NW/TiO_2 nanostructure as well as a typical ZnO NW/TiO_2-GO (10%) nanostructure is shown in Fig. 8(c) and 8(d), respectively. In the case of GO, a single XRD peak can be seen (Fig. 8(e)) at $2\Theta \sim 10.6^0$. This diffraction peak is caused by reflections from the (001) plane of the crystal surfaces [47].

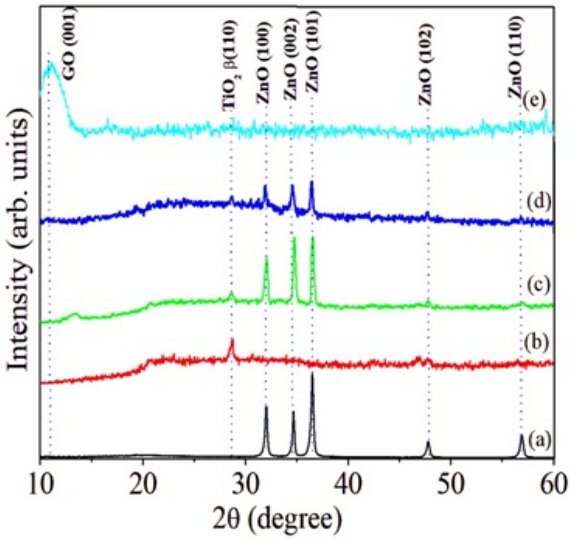

Fig. 8. The X-ray diffraction (XRD) pattern of the thin film is made up of (a) ZnO Nanowires (ZnO NWs), (b) pure TiO_2, (c) ZnO NW/TiO_2, (d) ZnO NW/TiO_2-GO (10%), and (e) GO nanoflakes.

4.3 ZnO NW/TiO_2-GO photo-anode based dye-sensitized solar cells

The J-V curves for the ZnO NW, ZnO NW/TiO_2, and ZnO NW/TiO_2-GO photo-anode based DSSC structures are shown in Fig. 9. A conventional DSSC structure is fabricated consisting of this hybrid structure as photo-anode, ruthenium based N3 dye as photosensitizers, iodine solution (I^-/I_3^+) as electrolyte and fluorine-doped tin oxide (FTO) coated glass substrate as counter electrode. From the J-V curve, we can determine that the open circuit voltage (V_{oc}) and short-circuit current density (J_{sc}) for ZnO NW are ~ 412 mV and ~ 1.01 mA/cm^2 respectively. A thin coating of TiO_2 on top of ZnO NW increases its V_{oc} and J_{sc} values to ~ 462 mV and 1.46 mA/cm^2, respectively. When a little amount of GO is progressively added to it, there is an enhancement in both the V_{oc} and J_{sc} values that are noticed. For a ZnO NW/TiO_2-GO (10%) based DSSC structure, the maximum values for V_{oc} and J_{sc} are recorded to be 491 mV and 2.19 mA/cm^2,

respectively. This is because the presence of GO facilitates the collection of electrons from the conduction band of TiO_2, hence minimizing the recombination loss [41]. When the percentage of GO in the composite is increased to 15%, the values obtained for V_{oc} and J_{sc} are 485 mV and 2.86 mA/cm^2, respectively. The V_{oc} ,J_{sc} and η values for a variety of samples are presented in Table-V. It has been shown that the ZnO NW/TiO_2-GO hybrid structure results in a significant improvement in FF values in comparison to ZnO NW or ZnO NW/TiO_2 based DSSC structures. In the ZnO NW/TiO_2-GO (10%) based DSSC structure, the maximum value of power conversion efficiency (η ~ 0.72 %) is obtained.

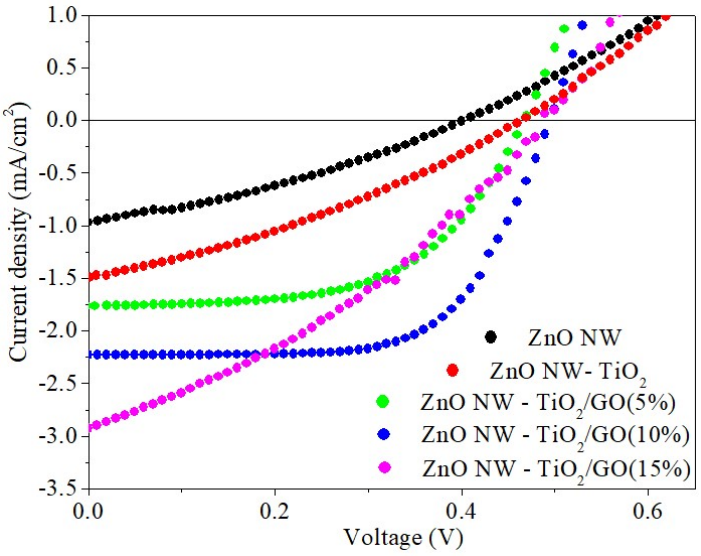

Fig. 9. The J-V curves for the hybrid nanostructures composed of ZnO NW-TiO_2/GO under illumination

Table- V: Characteristic parameters of different photo-anode based DSSCs estimated from J-V curves

Sample	V_{OC} (mV)	J_{SC} (mA/cm^2)	FF	η (%)	R_s (Ω)	R_{sh} (Ω)
ZnO NW	412	1.01	0.33	0.13	478.17 ± 7.36	2382.81 ± 5.64
ZnO NW/TiO_2	462	1.46	0.33	0.22	453.05 ± 3.31	3427.17 ± 5.80
ZnO NW-TiO_2-GO (5 %)	469	1.79	0.56	0.47	154.52 ± 1.25	4523.41 ± 7.41
ZnO NW-TiO_2-GO (10 %)	491	2.19	0.66	0.72	227.39 ± 3.12	4736.74 ± 9.50
ZnO NW-TiO_2-GO (15 %)	485	2.86	0.36	0.50	46.19 ± 0.62	1687.85 ± 3.39

Conclusion

We have synthesized and characterized the highly transparent TiO_2-GO nanocomposite thin films by sol-gel spin coating technique. Enhanced UV photoconductivity with GO incorporation in pristine TiO_2 thin film is attributed to the grain boundary modification by GO as evident from the detailed complex impedance analysis of TiO_2-GO nanocomposite thin films. When applied as the photo-anode of a basic dye-sensitized solar cell structure, the power conversion efficiency increased with the GO loading in the nanocomposite thin films. A hybrid structure comprised of vertically aligned ZnO nanowires coated with highly transparent TiO_2-GO nanocomposite demonstrated enhanced power conversion efficiency compared to bare ZnO nanowire, when used as the photo-anode of DSSC. Also the role of GO on the device parameters are studied critically, to come up with better understanding for the use of these metal oxide-graphene oxide nanocomposites for transparent optoelectronic devices.

References-

[1] H. ohta, M. Kamiya, T. Kamiya, M. Hirano, H. Hosono, UV-detector based on pn-heterojunction diode composed of transparent oxide semiconductors, p-NiO/n-ZnO, Thin Solid Films. 445(2) (2003) 317-321, https://doi.org/10.1016/S0040-6090(03)01178-7

[2] H. Yaghoubi, N. Taghavinia, E. K. Alamdari, Self-cleaning TiO_2 coating on polycarbonate: surface treatment, photocatalytic and nanomechanical properties, Surf. Coat. Technol. 204(9– 10) (2010) 1562–1568, https://doi.org/10.1016/j.surfcoat.2009.09.085

[3] J. Lin, Y. U. Heo, A. Nattestad, Z. Sun, L. Wang, J. H. Kim and S. X. Dou, 3D hierarchical rutile TiO_2 and metal-free organic sensitizer producing dye-sensitized solar cells 8.6% conversion efficiency, Sci. Rep. 4(1) (2014) 5769, https://doi.org/10.1038/srep05769

[4] M. Dadkhah, M. S. Niasari, N. Mir, Synthesis and characterization of TiO_2 nanoparticles by using new shape controllers and its application in dye sensitized solar cells. J. Ind. Eng. Chem. 20(6) (2014) 4039–4044, https://doi.org/10.1016/j. jiec.2014.01.003

[5] M. Sabet, M. S. Niasari, Deposition of cadmium selenide semiconductor nanostructures on TiO_2 surface via different chemical methods and investigation of their effects on dye sensitized solar cell efficiency,Mater.Sci.Semicond. Process. 27 (2014) 619–633, https://doi.org/10.1016/j.mssp.2014.07.031

[6] D. Nunes, A. Pimentel, J. Pinto, T. Calmeiro, S. Nandy, P. Barquinha, L. Pereira, P. A. Carvalho, E. Fortunato, R. Martins, Photocatalytic behavior of TiO_2 films synthesized by microwave irradiation, Catal. Today. 278(2) (2016) 262–270, https://doi.org/10.1016/j.cattod.2015.10.038

[7] D. Nunes, A. Pimentel, L. Santos, P. Barquinha, E. Fortunato, R. Martins, Photocatalytic TiO_2 nanorod spheres and arrays compatible with flexible applications, Catalysts. 7(12) (2017) 60, https://doi.org/10.3390/catal7020060

[8] I. B. Wojcik, R. Senadeera, P. J. Wojcik, L. B. Silva, G. Doria, P. Baptista, H. Aguas, E. Fortunato, R. Martins, Inkjet printed and "doctor blade" TiO_2 photodetectors for DNA biosensors, Biosens. Bioelectron. 25(5) (2010) 1229–1234, https://doi. org/10.1016/j.bios.2009.09.027

[9] J. Bai, B. Zhou, Titanium dioxide nanomaterials for sensor applications, Chem. Rev. 114(19) (2014) 10131–10176, https://doi. org/10.1021/cr400625j

[10] B. O' Regan and M. Gratzel, A low-cost high efficiency solar cell based on Dye- Sensitized colloidal TiO_2 films, Nature. 353 (1991) 737–740, https://doi.org/10.1038/353737a0

[11] S. Xuhui, C. Xinglan, T. Wanquan, W. Dong, and L. Kefei, Performance comparison of dye-sensitized solar cells by using different metal oxide coated TiO_2 as the photo anode, AIP Adv. 4(3) (2014) 031304, https://doi.org/10.1063/1.4863295

[12] N. G. Park, J. V. Lagemaat, and A. J. Frank, Comparison of dye sensitized rutile and anatase based TiO_2 solar cells, J. Phys. Chem. B. 104(38) (2000) 8989–8994, https://doi.org/10.1021/jp9943651

[13] J. Gupta, K. C. Barick, D. Bahadur, Defect mediated photocatalytic activity in shape-controlled ZnO nanostructures, J Alloys Compd. 509(23) (2011) 6725–6730,

https://doi.org/10.1016/j.jallcom.2011.03.157

[14] R. Paul, R. N. Gayen, S. Biswas, S. V. Bhat and R. Bhunia, Enhanced UV detection by transparent graphene oxide/ZnO composite thin films, RSC Adv. 6(66) (2016) 61661-61672, https://doi.org/10.1039/C6RA05039E

[15] D. Zhang, X. Gu, F. Jing, F. Gao, J. Zhou, S. Ruan, High performance ultraviolet detector based on TiO_2/ZnO heterojunction, J Alloys Compd. 618 (2015) 551-554,
https://doi.org/10.1016/j.jallcom.2014.09.004

[16] E. Akman, Enhanced photovoltaic performance and stability of dye-sensitized solar cells by utilizing manganese-doped ZnO photo-anode with europium compact layer, J. Mol. Liq. 317 (2020) 114223, https://doi.org/10.1016/j.molliq.2020.114223

[17] S. K. Wallace, K. P. Mckenna, Grain Boundary Controlled Electron Mobility in Polycrystalline Titanium Dioxide, Adv. Mater. Interfaces, 1(5) (2014) 1400078, https://doi.org/10.1002/admi.201400078

[18] J. Wang, G. Wang, J. Jiang, Z. Wan, Y. Su, H. Tang, Insight into charge carrier separation and solar-light utilization: rGO decorated 3D ZnO hollow microspheres for enhanced photocatalytic hydrogen evolution, J. Colloid Interface Sci. 564 (2020) 322-332, https://doi.org/10.1016/j.jcis.2019.12.111

[19] Y. Yang, L. Ren, C. Zhang, S. Huang and T. Liu, Facile fabrication of functionalized Graphene sheets (FGS)/ZnO nanocomposites with photocatalytic property, ACS Appl. Mater. Interfaces. 3(7) (2011) 2779–2785, https://doi.org/10.1021/am200561k

[20] R. Paul, F. Du, L. Dai, Y. Ding, Z.L. Wang, F. Wei, A. Roy, 3D heteroatom-doped carbon nanomaterials as multifunctional metal-free catalysts for integrated energy devices, Adv. Mater.31(13) (2019)1805598, https://doi.org/10.1002/adma.201805598

[21] H. Chang, H. Wu, Graphene-based nanocomposites: preparation,functionalization, and energy and environmental applications, Energy Environ. Sci. 6(12) (2013) 3483-3507, https://doi.org/10.1039/c3ee42518e

[22] E. S. Kadir, R. N. Gayen, R. Paul, S. Biswas, Interfacial effects on ferroelectric and dielecric properties of GO reinforced free-standing and flexible PVDF/ZnO composite membranes: Bias dependent impedance spectroscopy, J. Alloys Compd. 843 (2020) 155974, https://doi.org/10.1016/j.jallcom.2020.155974

[23] Y. Lin, X. Sun, D. S. Su, G. Centi, S. Perathoner, Catalysis by hybrid sp2 /sp3 nanodiamonds and their role in the design of advanced nanocarbon materials, Chem. Soc. Rev. 47 (2018) 8438, https://doi.org/10.1039/c8cs00684a

[24] M. Razeghi, A. Rogalski, Semiconductor ultraviolet detectors, J. Appl. Phys. 79(10) (1996) 7433-7473, https://doi.org/10.1063/1.362677

[25] Q. Wan, Q. H. Li, Y. J. Chen and T. H. Wang, Fabrication and ethanol sensing characteristics of ZnO nanowire gas sensors, Appl. Phys. Lett. 84(18) (2004) 3654-3656, https://doi.org/10.1063/1.1738932

[26] K. Liu, M. Sakurai, M. Aono, ZnO-based ultraviolet photodetectors, Sensors. 10(9) (2010) 8604-8634, https://doi.org/10.3390/s100908604

[27] C. Soci, A. Zhang, B. Xiang, S.A. Dayeh, D.P.R. Aplin, J. Park, X.Y. Bao, Y.H. Lo, D. Wang, ZnO nanowire UV photodetectors with high internal gain, NanoLett. 7 (2007) 1003, https://doi.org/10.1021/nl070111x

[28] E. Monroy, F. Omnes, and F. Calle, Wide-bandgap semiconductor ultraviolet Photodetectors, Semicond. Sci. Technol. 18 (2003) R33-R51, https://doi.org/10.1088/0268-1242/18/4/201

[29] D. B. Alwan and F. H. Ali, Hybrid TiO_2/ZnO nanopowder for several Dyes Sensitized Solar Cell, Int. j. sci. res. 6 (2017) 1609 – 1615, https://doi.org/10.21275/ART20176256

[30] L. T. Yan, F. L. Wu, L. Peng, L. J. Zhang, P. J. Li, S. Y. Dou, and T. X. Li, Photo-anode of Dye-Sensitized Solar Cells Based on a ZnO/TiO_2 Composite Film, Int. J. Photoenergy. 613969 (2012) 1-4, https://doi.org/10.1155/2012/613969

[31] M. Sookhakian, Y. M. Amin, S. Baradaran, M. T. Tajabadi, A. M. Golsheikh, W. J. Basirun, A layer-by-layer assembled graphene/zinc sulfide/polypyrrole thin-film electrode via electrophoretic deposition for solar cells, Thin Solid Films. 552 (2014) 204–211, https://doi.org/10.1016/j.tsf.2013.12.019

[32] A. S. Alshammari, M. M. Halim, F. K. Yam, N. H. M. Kaus, Effect of precursor concentration on the performance of UV photodetector using TiO_2/reduced graphene oxide (rGO) nanocomposite, Results Phys. 19 (2020) 103630, https://doi.org/10.1016/j.rinp.2020.103630

[33] D. Konatham, and A. Striolo, Molecular design of stable graphene nanosheets dispersions. Nano Lett. 8(12) (2008) 4630-4641, https://doi.org/10.1021/nl802262p

[34] Z. Zhu, F. Guo, Z. Xu, X. Di and Q. Zhang, Photocatalytic degradation of an organophosphorus pesticide using a ZnO/rGO composite, RSC Adv. 10 (2020) 11929-11938, https://doi.org/10.1039/D0RA01741H

[35] Z. Wang, H. Wang, B. Liu, W. Qiu, J. Zhang, S. Ran, H. Huang, J. Xu, H. Han, D. Chen, G. Shen, Transferable and flexible nanorod-assembled TiO_2 cloths for dye sensitized solar cells, photodetectors, and photocatalysts, ACS nano. 5(10) (2011) 8412-8419, https://doi.org/10.1021/nn203315k

[36] Y. Han, G. Wu, H. Li, M. Wang and H. Chen, Highly efficient ultraviolet photodetectors based on TiO_2 nanocrystal–polymer composites via wet processing, Nanotechnology. 21(18) (2010) 185708, https://doi.org/10.1088/0957-4484/21/18/185708

[37] S. Mahalingam, F. W. Low, A. Omar, A. Manap, N. A. Rahim, C. H. Tan, H. Abdullah, C. H. Voon, M. Rokhmat, E. Wibowo and C. S. Oon, Zinc oxide/graphene nanocomposite as efficient photoelectrode in dye-sensitized solar cells: Recent advances and future outlook, Int. J. Energy Res. 46(6) (2022) 7082-7100, https://doi.org/10.1002/er.7722

[38] L. Wei, P. Wang, Y. Yang, Z. Zhan, Y. Dong, W. Song and R. Fan, Enhanced performance of the dye-sensitized solar cells by the introduction of graphene oxide into the TiO_2 photo-anode, Inorg. Chem. Front. 5(1) (2018) 54-62, https://doi.org/10.1039/C7QI00503B

[39] J. Yu, X. Zhao, Q. Zhao, Photocatalytic activity of nanometer TiO_2 thin films prepared by the sol–gel method, Mater. Chem. Phys. 69 (1–3) (2001) 25–29, https://doi.org/10.1016/S0254-0584(00)00291-13

[40] T. Vasuki, D. Manickam, M. Venkatachalam, and S. Shanmugam, Preparation and characterization of TiO_2 thin films by spin coating method, J. Nanosci. Nanotechnol. 2(6) (2014) 728–731,

[41] R Paul, R N Gayen, S Biswas, S V Bhatt, R Bhunia, Enhanced UV detection by transparent graphene oxide/ZnO composite thin films, RSC Adv. 6 (2016) 61661–61672, https://doi.org/10.1039/C6RA05039E

[42] D.W. Scott, Y. Alseiha, Determining detection limits of aqueous anions using electrochemical impedance spectroscopy, J. Anal. Sci. Technol. 8 (1) (2017) 17, https://doi.org/10.1186/s40543-017-0126-9

[43] N.B. Saber, A. Mezni, A. Alrooqi, T. Altalhi, Fabrication of efficient Au@TiO_2/rGO heterojunction nanocomposite: boosted photocatalytic activity under ultraviolet and visible light irradiation, J. Mater. Res. Technol. 12 (2021) 2238–2246, https:// doi.org/10.1016/j.jmrt.2021.03.109

[44] A. S. Bondarenko, G. A. Ragoisha, in: A. L. Pomerantsev (Ed.), Application of a Coaxial-like Sensor for Impedance Spectroscopy Measurements of Selected Low-Conductivity Liquids, Progress in Chemometrics Research, Nova Science Publishers, New York, (2005) 89-102 https://doi.org/10.3390/s131013301

[45] J. E. A. M. van den Meerakker, J. J. Kelly, P. H. L. Notten, The Minority Carrier Recombination Resistance: A Useful Concept in Semiconductor Electrochemistry, J. Electrochem. Soc. 132 (1985) 638, https://doi.org/10.1149/1.2113920

[46] W. Hwang, E. Poon, H. C. Card, Carrier recombination at grain boundaries and the effective recombination velocity, Solid State Electron. 26, 6 (1983) 599 – 603, https://doi.org/10.1016/0038-1101(83)90175-2

[47] Y. Chen, X. Dong, Y. Cao, J. Xiang, H. Gao, Enhanced photocatalytic activities of low-bandgap TiO2-reduced graphene oxide nanocomposites, J. Nanopart. Res. 19 (2017) 200, https://doi.org/10.1007/s11051-017-3871-1

[48] R. N. Gayen and S. R. Bhattacharyya, Electrical characteristics and rectification performance of wet chemically synthesized vertically aligned n-ZnO nanowire/p-si heterojunction, J. Phys. D: Appl. Phys. 49 (11) (2016) 115102, https://doi.org/10.1088/0022-3727/49/11/115102

[49] J. Yu, X. Zhao, Q. Zhao, Photocatalytic activity of nanometer TiO_2 thin films prepared by the sol–gel method, Mater. Chem. Phys. 69 (1-3) (2001) 25 – 29, https://doi.org/10.1016/S0254-0584(00)00291-13